Research Square

Preprints are preliminary reports that have not undergone peer review.
They should not be considered conclusive, used to inform clinical practice,
or referenced by the media as validated information.

# Context-dependent regulation of malignant phenotypes by PCK1 in oral squamous cell carcinoma and its association with lactate- related transcriptomic features

**Yilidanna Dilixiati**
First Affiliated Hospital of Xinjiang Medical University
**Sagyndyk Zhumatay**
Zhongshan Hospital
**Maimaitituxun Tuerdi**
Dr.maimaitituxun@aliyun.com

First Affiliated Hospital of Xinjiang Medical University

**Research Article**

**Keywords:** PCK1, oral squamous cell carcinoma, lactate-related signature, metabolic reprogramming, tumor microenvironment, PI3K/Akt signaling

**Posted Date:** September 28th, 2026

**DOI:** https://doi.org/10.21203/rs.3.rs-10921386/v1

**License:** This work is licensed under a Creative Commons Attribution 4.0 International License. Read Full License

**Additional Declarations:** No competing interests reported.

## Abstract

# Background

Metabolic reprogramming and lactate-associated microenvironmental remodeling are integral to oral squamous cell carcinoma (OSCC) progression. Phosphoenolpyruvate carboxykinase 1 (PCK1), a cytosolic cataplerotic enzyme linking tricarboxylic-acid-cycle intermediates to phosphoenolpyruvate production, has context-dependent functions across malignancies. Its biological role and relationship with lactate-related transcriptional states in OSCC remain incompletely defined.

# Methods

A lactate-related prognostic signature was developed from TCGA-HNSC transcriptomic data using differential-expression analysis, univariable Cox regression, and LASSO-Cox modeling. PCK1 expression was evaluated by immunohistochemistry in 23 primary OSCC specimens and 15 non-malignant oral mucosal specimens. Functional effects were assessed in SCC25 and HSC3 cells using CCK-8, colony-formation, EdU-incorporation, wound-healing, and Transwell assays. A four-group SCC25-derived xenograft model (sh-PCK1, shNC, Vector, and OE-PCK1) was used to examine bidirectional PCK1 manipulation in vivo. Pathway associations were explored using GO/KEGG, GSEA/GSVA, immune-infiltration analyses, and tumor-tissue immunoblotting.

# Results

A total of 135 differentially expressed lactate-related genes were identified; 15 were associated with prognosis, and six genes (ABCB1, AKAP12, PCK1, PDGFA, SHCBP1, and SLC20A1) were retained in the final prognostic signature. The high-risk state was associated with shorter overall survival, lower stromal/immune/ESTIMATE scores, and distinct inferred immune-cell profiles. PCK1 expression was reduced in OSCC and was associated with adverse clinicopathological features and shorter overall survival. In vitro, PCK1 overexpression consistently reduced cellular viability, clonogenicity, DNA synthesis, migration, and invasion in SCC25 and HSC3 cells. In vivo, bidirectional PCK1 manipulation produced non-linear changes in tumor burden, Ki67, TUNEL, and total PI3K abundance, indicating that the phenotypic output of PCK1 is strongly conditioned by the tumor environment. Transcriptomic enrichment and xenograft protein data converged on a functional association with PI3K/Akt-related signaling.

# Conclusion

PCK1 is a clinically relevant metabolic regulator in OSCC that exerts a reproducible suppressive effect on malignant phenotypes in vitro while displaying context-dependent behavior in vivo. Its integration within a lactate-related transcriptional program associated with immune contexture and PI3K/Akt-related signaling identifies PCK1 as a biologically informative node linking carbon metabolism, tumor-cell behavior, and the microenvironment.

## Introduction

Oral squamous cell carcinoma (OSCC) is the predominant histological subtype of oral malignancy and remains a major clinical challenge because of local invasion, cervical lymph-node metastasis, recurrence, and treatment resistance [1–7]. Despite advances in surgery, radiotherapy, systemic therapy, and multidisciplinary care, outcomes for advanced and recurrent disease remain suboptimal. The marked biological heterogeneity of OSCC limits the

resolution of conventional clinicopathological staging and reinforces the need for molecular determinants that connect tumor-cell intrinsic programs with the surrounding tumor microenvironment (TME).

Metabolic reprogramming is increasingly recognized as a functional component of this heterogeneity. Enhanced aerobic glycolysis, altered mitochondrial substrate utilization, and dynamic metabolite exchange reshape both tumor-cell behavior and the TME [8, 10–15]. Lactate is particularly important because it can function simultaneously as a carbon source, redox-coupled metabolite, extracellular acidifying agent, and signaling molecule. Lactate-rich states can influence angiogenesis, immune-cell polarization, cellular plasticity, and treatment response [10–15]. Accordingly, a lactate-related transcriptional program may capture a coordinated metabolic-microenvironmental state that extends beyond the activity of any single metabolic enzyme.

PCK1 encodes the cytosolic isoform of phosphoenolpyruvate carboxykinase, which converts oxaloacetate to phosphoenolpyruvate and thereby governs a major cataplerotic step linking the tricarboxylic acid cycle to gluconeogenesis and biosynthetic carbon flow [16–22]. Cancer studies increasingly indicate that PCK1 is not a fixed oncogene or tumor suppressor; instead, its phenotypic output depends on lineage, nutrient availability, metabolic demand, expression level, and upstream regulatory context [18–22]. Importantly, an independent oral-cancer study demonstrated that PCK1 overexpression can partially restore malignant phenotypes after SRSF9 depletion, emphasizing that PCK1 function in oral cancer may vary according to the surrounding genetic and metabolic state [9].

We therefore hypothesized that the biological output of PCK1 in OSCC is conditioned by the broader lactate-related transcriptional and signaling environment. To address this hypothesis, we integrated TCGA-HNSC transcriptomic analysis, institutional tissue validation, in vitro functional assays in two OSCC cell lines, and bidirectional PCK1 manipulation in a xenograft model. The study was designed to define the prognostic landscape of a lactate-related molecular program, characterize the effects of PCK1 on malignant phenotypes, and explore pathway-level connections between PCK1-dependent metabolic state and PI3K/Akt-related signaling.

## Materials and methods

# Public transcriptomic data acquisition and preprocessing

RNA-sequencing data for The Cancer Genome Atlas Head and Neck Squamous Cell Carcinoma project (TCGA-HNSC; project record: https://portal.gdc.cancer.gov/projects/TCGA-HNSC; accessed 6 May 2024) were obtained from the Broad GDAC Firehose standard-data run dated 28 January 2016. Specifically, we used the Level 3 Illumina HiSeq RNA-seq V2 RSEM genes-normalized data product, Merge_rnaseqv2__illuminahiseq_rnaseqv2__unc_edu__Level_3__RSEM_genes_normalized__data (analysis build 2016012800.0.0; direct archive: https://gdac.broadinstitute .org/runs/stddata__latest/data/HNSC/20160128/gdac.broadinstitute.org_HNSC.Merge_rnaseqv2__illuminahiseq_rnaseqv2__unc_edu__Level_3__RSEM_genes_normalized__data.Level_3.2016012800.0.0.tar.gz). The downloaded matrix comprised 566 RNA-seq aliquots: 520 primary-tumor, 2 metastatic-tumor, and 44 solid-tissue normal samples. Clinical annotations were obtained from the cBioPortal Head and Neck Squamous Cell Carcinoma (TCGA, Firehose Legacy) study (study ID: hnsc_tcga; direct record: https://www.cbioportal.org/study/summary?id=hnsc_tcga). Overall-survival time and status were defined from OS_MONTHS and OS_STATUS, respectively. The supplied clinical table contained 528 patients; 520 primary-tumor cases matched the expression matrix, and 519 had non-missing overall-survival time before any further analytic exclusions. The supplied merged lactate- and hypoxia-related candidate list contained 764 unique gene symbols. After differential-expression screening, 135 genes formed the reported overlap used for downstream analysis.

Differential-expression analysis between tumor and non-malignant tissues was performed using the limma package in R. Genes with |log2 fold change| > 1 and $P < 0.05$ were considered differentially expressed; the Benjamini-Hochberg procedure was applied to high-dimensional comparisons where appropriate.

## Prognostic signature construction and molecular clustering

Univariable Cox proportional-hazards regression was used to identify lactate-related genes associated with overall survival (OS). Candidate prognostic genes were subsequently entered into least absolute shrinkage and selection operator (LASSO) Cox regression to reduce dimensionality and construct a multigene signature. The risk score was calculated as the sum of the expression level of each retained gene multiplied by its corresponding LASSO-Cox coefficient. Patients were stratified into high- and low-risk groups using the median risk score. Kaplan-Meier analysis, log-rank testing, and time-dependent receiver operating characteristic (ROC) curves were used to assess prognostic separation and discrimination.

Unsupervised consensus clustering was performed using ConsensusClusterPlus [23] to identify lactate-related molecular subgroups. Cluster stability was evaluated across repeated subsampling iterations, and survival differences between molecular states were examined by Kaplan-Meier analysis. A prognostic nomogram integrating the risk score with available clinicopathological variables was generated as an individualized representation of OS probability.

## Functional enrichment and immune-infiltration analysis

Gene Ontology (GO) and Kyoto Encyclopedia of Genes and Genomes (KEGG) enrichment analyses were used to characterize biological functions and pathway associations. Gene Set Enrichment Analysis (GSEA) [24] and Gene Set Variation Analysis (GSVA) [25] were further used to examine pathway-level differences associated with the lactate-related risk state and PCK1 expression.

The tumor immune microenvironment was computationally characterized using established transcriptome-deconvolution and scoring approaches, including CIBERSORT [26], ESTIMATE, and complementary immune-infiltration algorithms. StromalScore, ImmuneScore, ESTIMATEScore, inferred immune-cell fractions, and immune-related features were compared between risk groups, and correlations with the risk score were evaluated.

## Human tissue specimens and immunohistochemistry

A total of 23 primary OSCC specimens and 15 non-malignant oral mucosal specimens were collected from patients treated at the First Affiliated Hospital of Xinjiang Medical University. All OSCC specimens were histopathologically confirmed. Non-malignant oral mucosa was obtained from excess tissue removed during routine oral surgical procedures and was histologically confirmed to contain non-malignant epithelium.

PCK1 protein expression was evaluated by immunohistochemistry (IHC). Five representative microscopic fields were assessed for each specimen. Digital images were analyzed using ImageJ, and PCK1 staining was quantified as integrated optical density (IOD) relative to the corresponding stained area; mean staining density was used to represent relative tissue expression.

The human-tissue study was approved by the Ethics Committee of the First Affiliated Hospital of Xinjiang Medical University (approval no. 240522-35). Written informed consent was obtained from all participants. All procedures

involving human participants and human tissue were performed in accordance with the Declaration of Helsinki and applicable national requirements.

## Cell culture and PCK1 manipulation

Human SCC25 cells were obtained from Procell Life Science & Technology Co., Ltd. (Wuhan, China; cat. no. CL-0569; https://www.procell.com.cn/p/scc-25-scc-25-scc25-cl-0569-68657), and HSC3 cells were obtained from Shanghai Yaji Biotechnology Co., Ltd. (Shanghai, China; cat. no. YS1645C; https://www.yajimall.com/product/detail/9751.html). SCC25 cells were cultured in DMEM/F12 supplemented with 10% fetal bovine serum, 1% penicillin-streptomycin, and hydrocortisone; HSC3 cells were cultured in MEM supplemented with 10% fetal bovine serum and 1% penicillin-streptomycin. Cells were maintained at 37°C in a humidified atmosphere containing 5% CO2.

Stable PCK1 overexpression was established in SCC25 and HSC3 cells using lentiviral transduction. For the SCC25 model, 1.20 × 10^6 cells were seeded in a 10-cm dish and transduced at a multiplicity of infection of 15 in the presence of Polybrene. The empty-vector control was CON335 (1.80 × 10^9 TU/mL; 10.0 μL), and the PCK1-overexpression construct was LV-PCK1 KL60531-1 (1.70 × 10^9 TU/mL; 10.6 μL). Medium was replaced 16 h after transduction, followed by selection with 2.0 μg/mL puromycin for 48 h and maintenance in 1.0 μg/mL puromycin. PCK1-silenced SCC25 cells and their non-targeting controls were used for the bidirectional in vivo design.

# RT-qPCR and immunoblotting

Total RNA was extracted using TRIzol reagent, and complementary DNA was synthesized with M-MLV reverse transcriptase. Quantitative real-time PCR was performed using SYBR Premix Ex Taq on a LightCycler 480 II system. ACTB served as the internal reference gene, and relative PCK1 expression was calculated using the 2^-ΔΔCt method. Primer sequences were: ACTB forward 5'-GCGTGACATTAAGGAGAAGC-3' and reverse 5'-CCACGTCACACTTCATGATGG-3'; PCK1 forward 5'-GCTGGTGTCCCTCTAGTCTATG-3' and reverse 5'-CAGGTATTTGCCGAAGTTGTAG-3'.

For PCK1-overexpression verification, 40 μg of total protein per lane was separated by SDS-PAGE and detected by enhanced chemiluminescence. Primary antibodies included anti-PCK1, anti-FLAG, and anti-β-actin. Xenograft tumor-tissue immunoblotting was used to assess PCK1, Ki67, total PI3K, and GAPDH abundance.

## In vitro functional assays

Cell viability was evaluated using the Cell Counting Kit-8 (CCK-8) assay at 12, 24, 48, and 72 h. CCK-8 reagent was added at each time point, cells were incubated for 2 h at 37°C, and absorbance was measured at 450 nm.

For colony formation, cells were seeded at low density in six-well plates and cultured for approximately 14 days. Colonies were fixed with 4% paraformaldehyde, stained with crystal violet, photographed, and counted. DNA synthesis was evaluated by EdU incorporation using 20 μM EdU for 2 h, followed by fixation, permeabilization, Click-reaction detection, Hoechst 33342 counterstaining, and quantification of EdU-positive nuclei.

For wound-healing assays, cells were cultured to near confluence, scratched with a sterile pipette tip, washed with PBS, and maintained in serum-free or low-serum medium. Images were obtained at 0, 12, and 24 h and analyzed using ImageJ. Migration and invasion were quantified using Transwell assays. Uncoated inserts were used for migration and Matrigel-coated inserts for invasion; medium containing 10% fetal bovine serum served as the chemoattractant. After 24 h, migrated or invaded cells were fixed, stained with crystal violet, and quantified in five microscopic fields.

## Xenograft tumor model and tissue analysis

Animal experiments were reviewed and approved by the Animal Experiment Medical Ethics Committee of the First Affiliated Hospital of Xinjiang Medical University (approval no. A240522-40) and were conducted in accordance with institutional animal-welfare requirements and ARRIVE 2.0 reporting principles [29]. Four- to six-week-old BALB/c nude mice weighing 18–22 g were obtained from the Laboratory Animal Center, Chongqing Brain and Intelligence Science Center (Chongqing, China).

Before subcutaneous inoculation and endpoint procedures, mice were anaesthetized with inhaled isoflurane (3–5% for induction and 1–2% for maintenance). Anaesthetic depth was monitored by respiratory pattern, loss of the corneal reflex, and absence of response to a noxious stimulus. SCC25-derived cells assigned to sh-PCK1, shNC, Vector, or OE-PCK1 groups were resuspended at $1 \times 10^7$ cells/mL, and 100 μL of cell suspension ($1 \times 10^6$ cells) was injected subcutaneously into the dorsal flank. Tumor length and width were measured with calipers, and volume was calculated as $V = (L \times W^2)/2$. At the experimental endpoint, mice were euthanized by carbon-dioxide inhalation while anaesthetized. Death was confirmed by permanent cessation of respiration and heartbeat and absence of the corneal reflex. Tumors and major organs (heart, liver, spleen, lung, and kidney) were collected. Tumor sections underwent H&E staining, TUNEL analysis, and IHC for PCK1 and Ki67; major organs underwent H&E examination. The prespecified construct-matched comparisons were sh-PCK1 versus shNC and OE-PCK1 versus Vector.

# Statistical analysis

Statistical analyses were performed using R for transcriptomic analyses and GraphPad Prism 9 for experimental data. Continuous experimental data are presented as mean ± standard deviation (SD) unless otherwise specified. Two-group comparisons were performed using two-sided unpaired Student's t tests where appropriate, and multigroup comparisons used one-way analysis of variance followed by appropriate post hoc testing. Survival curves were generated using the Kaplan-Meier method and compared by log-rank test. Cox regression, LASSO-Cox modeling, and time-dependent ROC analyses were performed in R. High-dimensional transcriptomic comparisons were adjusted using the Benjamini-Hochberg procedure where appropriate. All tests were two-sided, and $P < 0.05$ was considered statistically significant.

## Results

# Identification of a lactate-related prognostic signature in OSCC

Integration of the TCGA-HNSC expression profiles with the curated lactate-related gene set identified 135 differentially expressed lactate-related genes (Fig. 1A, B). Univariable Cox analysis identified 15 prognosis-associated genes, and LASSO-Cox modeling retained six genes—ABCB1, AKAP12, PCK1, PDGFA, SHCBP1, and SLC20A1—in the final prognostic signature (Fig. 1G, H). Patients were subsequently stratified into high- and low-risk groups according to the median risk score.

Consensus clustering based on the lactate-related prognostic program identified distinct molecular states with significantly different survival outcomes (log-rank $P = 0.007$; Fig. 1J). These results support biological heterogeneity within the lactate-associated transcriptional landscape of OSCC.

# Clinical and microenvironmental implications of the prognostic signature

Kaplan-Meier analyses showed shorter OS in the high-risk group, with displayed log-rank P values of 0.016, < 0.001, and < 0.001 across the evaluated cohort panels (Fig. 2B). Time-dependent ROC analysis yielded 1-, 3-, and 5-year OS AUCs of 0.630, 0.676, and 0.592, respectively. A nomogram integrating the risk score with available clinicopathological variables was generated to visualize individualized survival prediction (Fig. 2C).

Tumor-microenvironment analysis showed lower StromalScore, ImmuneScore, and ESTIMATEScore values in the high-risk group (Fig. 2E). The risk score correlated negatively with activated memory CD4 + T cells (R = -0.19, P = 0.00029), memory B cells (R = -0.14, P = 0.0064), and M1 macrophages (R = -0.12, P = 0.017; Fig. 2H), indicating that the lactate-related risk state was accompanied by a distinct inferred immune-cell composition.

GO, KEGG, GSEA, and GSVA analyses identified coordinated alterations in cancer-related and metabolic programs. PI3K/Akt-related signaling was prominent together with glycolysis/gluconeogenesis, pyruvate metabolism, and the citrate cycle (Fig. 2D, F), linking the prognostic program to central carbon metabolism and growth-factor signaling.

# PCK1 is downregulated in OSCC and correlates with aggressive disease

PCK1 expression was lower in tumor than in non-malignant transcriptomic profiles. Lower PCK1 expression was associated with shorter OS and with adverse clinicopathological characteristics, including lymph-node metastasis, perineural invasion, poorer differentiation, and advanced clinical stage. Consistently, IHC analysis of the institutional series (23 primary OSCC specimens and 15 non-malignant oral specimens) showed lower PCK1 protein staining in tumor tissue than in normal or paracancerous oral mucosa (Fig. 3A).

# PCK1 elicits a consistent tumor-suppressive phenotype in vitro

RT-qPCR and immunoblotting confirmed increased PCK1 transcript and protein abundance after lentiviral overexpression in SCC25 and HSC3 cells (Fig. 3B). PCK1-overexpressing cells showed lower CCK-8 values, markedly reduced colony formation, and decreased EdU incorporation compared with their corresponding controls (Fig. 3C-E), demonstrating suppression of proliferative and clonogenic phenotypes in both OSCC cell lines.

PCK1 overexpression also reduced cell motility and invasion. Wound-healing assays demonstrated impaired wound closure, and Transwell assays showed significantly fewer migrated and invaded SCC25 and HSC3 cells than in the corresponding control groups (Fig. 3F, G). The concordant results across two cell lines establish a reproducible inhibitory effect of PCK1 overexpression on major malignant cell phenotypes under standard in vitro conditions.

# PCK1 exhibits context-dependent in vivo behavior associated with PI3K/Akt-related signaling

Bidirectional PCK1 manipulation produced clear but non-linear changes in xenograft growth and tumor-cell state across the sh-PCK1, shNC, Vector, and OE-PCK1 groups (Fig. 4A-D). PCK1 IHC confirmed the expected direction of target manipulation. Endpoint tumor burden, Ki67 staining, and TUNEL positivity varied substantially among groups rather than reproducing a simple linear extension of the in vitro phenotype. This pattern indicates that the phenotypic output of PCK1 is strongly conditioned by the metabolic and signaling environment encountered in vivo.

Body weights were comparable across the four groups, and representative H&E sections of the heart, liver, spleen, lung, and kidney did not show overt treatment-associated histomorphological abnormalities (Fig. 4E). Tumor-tissue immunoblotting demonstrated group-dependent changes in PCK1, Ki67, and total PI3K abundance (Fig. 4F). Together

with the pathway-enrichment results, these data support an intersection between PCK1-dependent metabolic state and PI3K/Akt-related signaling while emphasizing that the relationship is context dependent in vivo.

## Discussion

This study integrates a lactate-related transcriptomic framework with clinical tissue validation and functional experimentation to define the biological position of PCK1 in OSCC. Three findings are particularly informative. First, a six-gene lactate-related program stratified patients by OS and was accompanied by distinct immune and metabolic pathway states. Second, PCK1 was reduced in OSCC and its lower expression was associated with adverse clinicopathological characteristics. Third, restoration of PCK1 generated a highly consistent suppressive phenotype across proliferation, clonogenicity, DNA synthesis, migration, and invasion in two independent OSCC cell lines, whereas bidirectional manipulation in xenografts produced a non-linear response. Taken together, these observations identify PCK1 as a metabolic regulator whose functional output is strong in vitro but modulated by the in vivo tumor environment.

The biological interpretation of PCK1 is therefore better framed as metabolic context dependence than as a fixed oncogenic or tumor-suppressive identity. PCK1 controls the conversion of oxaloacetate to phosphoenolpyruvate and thereby regulates cataplerotic carbon withdrawal from the TCA cycle [16–22]. Under standard culture conditions, increasing PCK1 activity may redistribute carbon away from anabolic intermediates required for rapid proliferation and motility, while influencing redox balance and biosynthetic flexibility. Such a mechanism is consistent with the broad suppression observed across CCK-8, colony formation, EdU, and Transwell assays. In contrast, a living tumor continuously experiences spatially heterogeneous glucose, glutamine, lactate, oxygen, stromal metabolites, and growth-factor signals. Under these conditions, the same metabolic enzyme can confer different advantages or liabilities depending on substrate availability and pathway demand. The context-dependent behavior reported for PCK1 across cancer types [18–22], together with the SRSF9-PCK1 rescue relationship described in oral cancer [9], supports this metabolic-rheostat model.

The lactate-related component of our analysis provides a broader framework for this context dependence. The high-risk transcriptional state was associated with lower stromal, immune, and ESTIMATE scores and with reduced inferred abundance of activated memory CD4 + T cells, memory B cells, and M1 macrophages. Lactate-associated states can reshape extracellular pH, redox balance, substrate exchange, angiogenesis, and immune-cell function [10–15]. The present signature should therefore be understood as a molecular representation of a coordinated metabolic-microenvironmental state rather than a surrogate for lactate concentration alone. Within that state, PCK1 may influence how carbon is partitioned between cataplerosis, glycolytic intermediates, mitochondrial metabolism, and biosynthesis, thereby linking tumor-cell metabolism to microenvironmental adaptation.

The enrichment of PI3K/Akt-related signaling provides a second mechanistic layer. PI3K/Akt signaling coordinates nutrient uptake, glycolysis, survival, biosynthesis, and therapy resistance, whereas PCK1 directly alters carbon-flow architecture. The convergence of pathway enrichment with changes in total PI3K abundance in xenograft tissue supports a functional intersection between these systems. One plausible model is that PCK1-dependent carbon redistribution alters the metabolic requirements and feedback signals that sustain PI3K/Akt pathway activity; conversely, growth-factor signaling may determine when PCK1-mediated cataplerosis is growth inhibitory or metabolically adaptive. This reciprocal metabolic-signaling interface offers a mechanistically testable explanation for why PCK1 produces a strong suppressive phenotype in controlled cell culture yet a more complex response in vivo.

The study also has translational implications. The six-gene signature links PCK1 to a broader disease state involving prognosis, immune contexture, and central carbon metabolism. Rather than positioning PCK1 as an isolated marker,

these findings support its evaluation as part of an integrated metabolic-risk framework and as a candidate node for mechanism-guided therapeutic studies. Experimental strategies combining PCK1 perturbation with PI3K/Akt inhibitors, nutrient-defined culture systems, and immune-competent or patient-derived models may help identify the biological contexts in which PCK1 manipulation is most therapeutically informative.

This study should be interpreted in light of several focused limitations. Direct lactate quantification, isotope-based metabolic-flux analysis, and metabolomic profiling were not included, so the lactate-related signature represents a transcriptional metabolic state rather than a direct measurement of lactate flux. In addition, the tumor-tissue protein analysis assessed total PI3K abundance; time-resolved phosphorylation measurements of AKT and mTOR, together with perturbation-rescue experiments, will be important for defining pathway directionality. Finally, the prognostic model was developed from public transcriptomic data and will benefit from evaluation in independent multi-center cohorts. These next steps are well aligned with the context-dependent model generated by the current findings.

## Conclusion

Our integrated findings identify PCK1 as a significantly downregulated metabolic regulator in OSCC that exerts reproducible suppressive effects on proliferation, clonogenicity, DNA synthesis, migration, and invasion in vitro. Its non-linear behavior after bidirectional manipulation in xenografts highlights the influence of the tumor microenvironment on metabolic-enzyme function. Positioned within a lactate-related molecular program associated with prognosis, immune contexture, and PI3K/Akt-related signaling, PCK1 represents a biologically informative node linking carbon metabolism to oral-cancer behavior and provides a strong rationale for future mechanistic studies of metabolism-signaling vulnerabilities in OSCC.

## Abbreviations

PCK1
phosphoenolpyruvate carboxykinase 1
OSCC
oral squamous cell carcinoma
TME
tumor microenvironment
TCGA
The Cancer Genome Atlas
OS
overall survival
LASSO
least absolute shrinkage and selection operator
ROC
receiver operating characteristic
GO
Gene Ontology
KEGG
Kyoto Encyclopedia of Genes and Genomes
GSEA
Gene Set Enrichment Analysis
GSVA

Gene Set Variation Analysis
IHC
immunohistochemistry
IOD
integrated optical density
CCK-8
Cell Counting Kit-8
TUNEL
terminal deoxynucleotidyl transferase dUTP nick-end labeling
PI3K
phosphatidylinositol 3-kinase.

## Declarations

Ethics approval and consent to participate

The human-tissue study was approved by the Ethics Committee of the First Affiliated Hospital of Xinjiang Medical University (approval no. 240522-35). Written informed consent was obtained from all participants. All procedures involving human participants and human tissue were performed in accordance with the Declaration of Helsinki and applicable national requirements. Animal experiments were reviewed and approved by the Animal Experiment Medical Ethics Committee of the First Affiliated Hospital of Xinjiang Medical University (approval no. A240522-40) and were conducted in accordance with institutional animal-welfare requirements.

Consent for publication

Not applicable.

Data availability

The RNA-sequencing dataset analyzed in this study was the Broad GDAC Firehose TCGA-HNSC Level 3 Illumina HiSeq RNA-seq V2 RSEM genes-normalized data product from the 28 January 2016 standard-data run (analysis build 2016012800.0.0; direct archive: https://gdac.broadinstitute.org/runs/stddata_ _latest/data/HNSC/20160128/gdac.broadinst itute.org_HNSC.Merge_rnaseqv2__illuminahiseq _rnaseqv2__unc_edu__Level_3__RSEM_genes_n ormalized__data.Level_3.2016012800.0.0.tar.gz). The underlying project accession is TCGA-HNSC (GDC project record: https://portal.gdc.cancer.gov/projects/TCGA-HNSC). Clinical annotations and overall-survival variables were obtained from the cBioPortal Head and Neck Squamous Cell Carcinoma (TCGA, Firehose Legacy) study (study ID: hnsc_tcga; direct record: https://www.cbioportal.org/study/summary?id=hnsc_tcga). The merged lactate- and hypoxia-related candidate list contained 764 unique gene symbols. De-identified data generated during the current study are available from the corresponding author on reasonable request, subject to institutional and ethical requirements.

Competing interests

The authors declare that they have no competing interests.

Funding

This work was supported by the National Natural Science Foundation of China (grant no. 82360198). The funder had no role in study design, data collection and analysis, interpretation of data, or writing of the manuscript.

CRediT authorship contribution statement

**Yilidanna Dilixiati:** Conceptualization, Methodology, Formal analysis, Investigation, Data curation, Writing—original draft. **Sagyndyk Zhumatay:** Conceptualization, Methodology, Investigation, Formal analysis, Visualization, Writing—original draft. **Maimaitituxun Tuerdi:** Conceptualization, Funding acquisition, Resources, Supervision, Validation, Writing—review and editing. All authors reviewed and approved the final manuscript and agreed to be accountable for all aspects of the work.

## References

1. Li C, Dong X, Li B. Tumor microenvironment in oral squamous cell carcinoma. Front Immunol. 2024;15:1485174. 10.3389/fimmu.2024.1485174.
2. Zou E, Venkatraman C, Sweeney J, Flannery K, Lailer S, Mehdiyar D, et al. Current and emerging protein biomarkers for the diagnosis and prognosis of head and neck cancer. Genes (Basel). 2025;16:1493. 10.3390/genes16121493.
3. Patel HV, Joshi JS, Shah FD. Implicating clinical utility of altered expression of PTCH1 & SMO in oral squamous cell carcinoma. J Mol Histol. 2024;55:379–89. 10.1007/s10735-024-10215-3.
4. Sundaram GA, Chokkattu JJ, Krishnan M, Kumar SP, Senthilmurugan M, Lakshmanan S. Lymph node ratio as a prognostic factor for oral tongue squamous cell carcinoma: a retrospective study. Cureus. 2023;15:e44109. 10.7759/cureus.44109.
5. Rajoria S, Kumar P, Kumar A, Aiyer HM, Rawat G, Urs AB. Immunohistochemical analysis of STAT3 and ITGB6 in oral squamous cell carcinoma: prognostic relevance for lymph node metastasis and overall survival. Appl Immunohistochem Mol Morphol. 2026;34:86–94. 10.1097/PAI.0000000000001309.
6. Li Y, Lin Y, Li X, Chen Y, Chen G, Yang H. A group of highly secretory miRNAs correlates with lymph node metastasis and poor prognosis in oral squamous cell carcinoma. Biomolecules. 2024;14:224. 10.3390/biom14020224.
7. Duan W, Wu Z, Mei X, Li J, Lu H, Liang Y, et al. Intratumoral platelet microthrombi in oral squamous cell carcinoma: a marker of lymph node metastasis. Oral Dis. 2024;30:2894–906. 10.1111/odi.14575.
8. Lazure F, Gomes AP. Cancer progression through the lens of age-induced metabolic reprogramming. Nat Rev Cancer. 2025;25:801–17. 10.1038/s41568-025-00845-4.
9. Peng Q, Wang L, Long Y, Tian H, Xu X, Ren Z, et al. SRSF9 mediates oncogenic RNA splicing of SLC37A4 via liquid-liquid phase separation to promote oral cancer progression. J Adv Res. 2026;79:505–20. 10.1016/j.jare.2025.03.013.
10. Cappellesso F, Mazzone M, Virga F. Acid affairs in anti-tumour immunity. Cancer Cell Int. 2024;24:354. 10.1186/s12935-024-03520-0.
11. Singh L, Nair L, Kumar D, Arora MK, Bajaj S, Gadewar M, et al. Hypoxia induced lactate acidosis modulates tumor microenvironment and lipid reprogramming to sustain the cancer cell survival. Front Oncol. 2023;13:1034205. 10.3389/fonc.2023.1034205.
12. Rastogi S, Mishra SS, Arora MK, Kaithwas G, Banerjee S, Ravichandiran V, et al. Lactate acidosis and simultaneous recruitment of TGF-β leads to alter plasticity of hypoxic cancer cells in tumor microenvironment. Pharmacol Ther. 2023;250:108519. 10.1016/j.pharmthera.2023.108519.

13. Wang M, Zhou Q, Cao T, Li F, Li X, Zhang M, et al. Lactate dehydrogenase A: a potential new target for tumor drug resistance intervention. J Transl Med. 2025;23:713. 10.1186/s12967-025-06773-z.
14. Wu P, Zhang J, Jiang Z, Liu X, Jiang N, Zou J, et al. Lactate-lactylation in tumor angiogenesis and progression: mechanisms, biomarker potential, and therapeutic implications. Biomark Res. 2026;14:21. 10.1186/s40364-026-00898-z.
15. Sun Y, Wang H, Cui Z, Yu T, Song Y, Gao H, et al. Lactylation in cancer progression and drug resistance. Drug Resist Updat. 2025;81:101248. 10.1016/j.drup.2025.101248.
16. Gonzalez-Rellan MJ, Fernández U, Parracho T, Novoa E, Fondevila MF, da Silva Lima N, et al. Neddylation of phosphoenolpyruvate carboxykinase 1 controls glucose metabolism. Cell Metab. 2023;35:1630. 45.e5.
17. Zhu XR, Peng SQ, Wang L, Chen XY, Feng CX, Liu YY, et al. Identification of phosphoenolpyruvate carboxykinase 1 as a potential therapeutic target for pancreatic cancer. Cell Death Dis. 2021;12:918. 10.1038/s41419-021-04201-w.
18. Xiang J, Wang K, Tang N. PCK1 dysregulation in cancer: metabolic reprogramming, oncogenic activation, and therapeutic opportunities. Genes Dis. 2023;10:101–12. 10.1016/j.gendis.2022.02.010.
19. Liu N, Zhu XR, Wu CY, Liu YY, Chen MB, Gu JH. PCK1 as a target for cancer therapy: from metabolic reprogramming to immune microenvironment remodeling. Cell Death Discov. 2024;10:478. 10.1038/s41420-024-02240-8.
20. Liu MX, Jin L, Sun SJ, Liu P, Feng X, Cheng ZL, et al. Metabolic reprogramming by PCK1 promotes TCA cataplerosis, oxidative stress and apoptosis in liver cancer cells and suppresses hepatocellular carcinoma. Oncogene. 2018;37:1637–53. 10.1038/s41388-017-0070-6.
21. Tuo L, Xiang J, Pan X, Hu J, Tang H, Liang L, et al. PCK1 negatively regulates cell cycle progression and hepatoma cell proliferation via the AMPK/p27Kip1 axis. J Exp Clin Cancer Res. 2019;38:50. 10.1186/s13046-019-1029-y.
22. Huang K, Han Y, Chen Y, Shen H, Zeng S, Cai C. Tumor metabolic regulators: key drivers of metabolic reprogramming and the promising targets in cancer therapy. Mol Cancer. 2025;24:7. 10.1186/s12943-024-02205-6.
23. Wilkerson MD, Hayes DN. ConsensusClusterPlus: a class discovery tool with confidence assessments and item tracking. Bioinformatics. 2010;26:1572–3. 10.1093/bioinformatics/btq170.
24. Subramanian A, Tamayo P, Mootha VK, Mukherjee S, Ebert BL, Gillette MA, et al. Gene set enrichment analysis: a knowledge-based approach for interpreting genome-wide expression profiles. Proc Natl Acad Sci U S A. 2005;102:15545–50. 10.1073/pnas.0506580102.
25. Hänzelmann S, Castelo R, Guinney J. BMC Bioinformatics. 2013;14:7. 10.1186/1471-2105-14-7. GSVA: gene set variation analysis for microarray and RNA-seq data.
26. Newman AM, Liu CL, Green MR, Gentles AJ, Feng W, Xu Y, et al. Robust enumeration of cell subsets from tissue expression profiles. Nat Methods. 2015;12:453–7. 10.1038/nmeth.3337.
27. Collins GS, Reitsma JB, Altman DG, Moons KGM. Transparent reporting of a multivariable prediction model for individual prognosis or diagnosis (TRIPOD): the TRIPOD statement. Ann Intern Med. 2015;162:55–63. 10.7326/M14-0697.
28. Bustin SA, Benes V, Garson JA, Hellemans J, Huggett J, Kubista M, et al. The MIQE guidelines: minimum information for publication of quantitative real-time PCR experiments. Clin Chem. 2009;55:611–22. 10.1373/clinchem.2008.112797.
29. Percie du Sert N, Hurst V, Ahluwalia A, Alam S, Avey MT, Baker M, et al. The ARRIVE guidelines 2.0: updated guidelines for reporting animal research. PLoS Biol. 2020;18:e3000410. 10.1371/journal.pbio.3000410.

# Figures

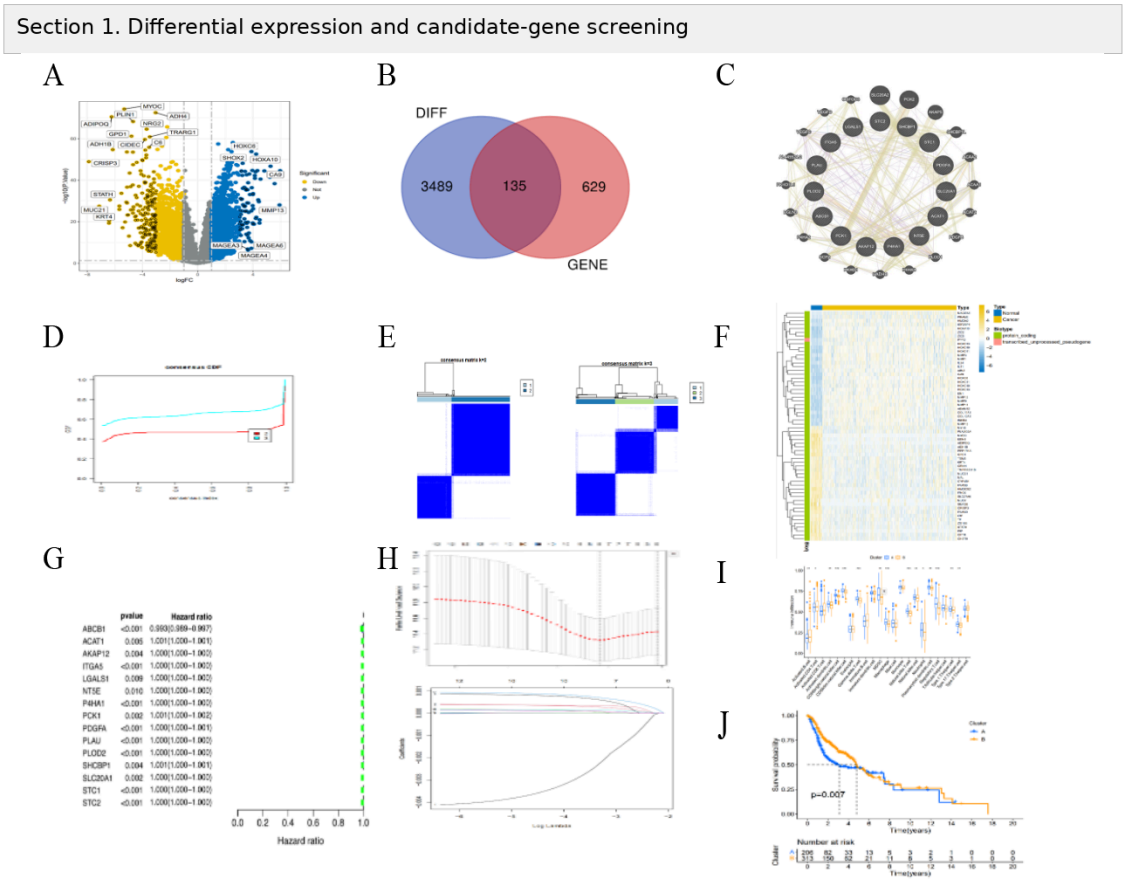



**Figure 1**

Bioinformatic identification of lactate-related genes, molecular subgroups, and construction of the six-gene prognostic signature. (A) Differential-expression analysis. (B) Overlap between differentially expressed and candidate lactate-related genes, yielding 135 genes. (C) Co-expression network. (D, E) Consensus-clustering distribution and consensus matrices. (F) Gene-expression and clinicopathological heatmap. (G) Univariable Cox-regression screening

of 15 prognosis-associated genes. (H) LASSO-Cox coefficient selection. (I) Expression patterns across molecular subgroups. (J) Kaplan-Meier comparison of molecular clusters (log-rank P = 0.007). (K) Risk-score distributions, OS status, and expression of ABCB1, AKAP12, PCK1, PDGFA, SHCBP1, and SLC20A1 across the modeling cohorts.

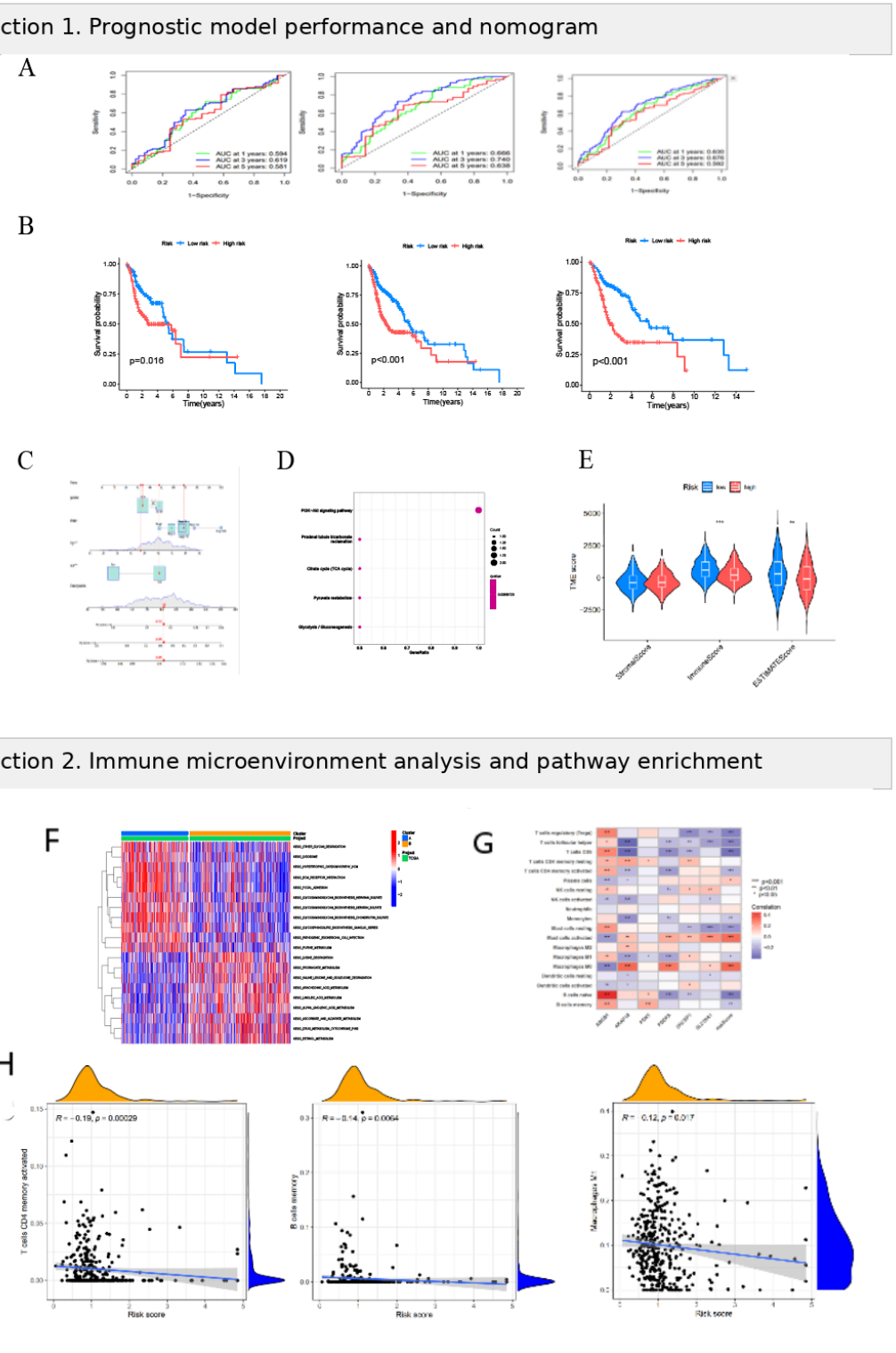



**Figure 2**

Prognostic performance, tumor-microenvironment characteristics, and pathway associations of the six-gene signature. (A) Time-dependent ROC curves. (B) Kaplan-Meier OS analyses comparing high- and low-risk groups. (C)

Prognostic nomogram. (D) Enrichment of PI3K/Akt-related and metabolic pathways, including citrate-cycle, pyruvate-metabolism, and glycolysis/gluconeogenesis terms. (E) StromalScore, ImmuneScore, and ESTIMATEScore distributions according to risk group. (F) Pathway-activity heatmap. (G) Correlations between signature-gene expression and inferred immune-cell fractions. (H) Correlations of the risk score with activated memory CD4+ T cells, memory B cells, and M1 macrophages.

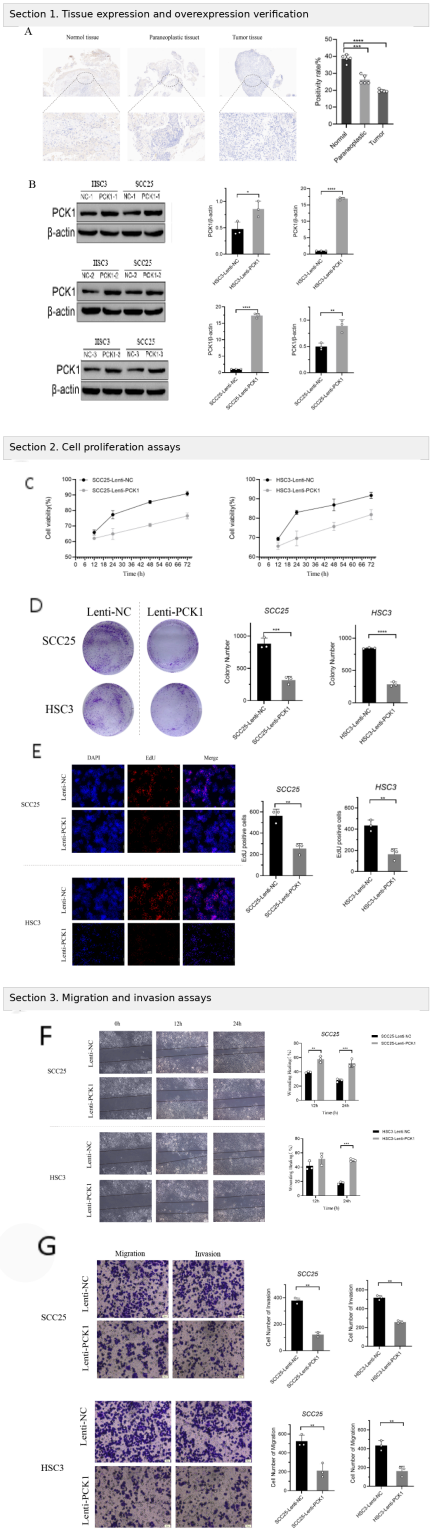



**Figure 3**

PCK1 expression in OSCC tissues and in vitro phenotypes following PCK1 overexpression. (A) PCK1 immunohistochemistry in normal, paracancerous, and tumor tissues. (B) Immunoblot and RT-qPCR verification of PCK1 overexpression in HSC3 and SCC25 cells. (C-E) CCK-8, colony-formation, and EdU-incorporation assays. (F) Wound-healing assay. (G) Transwell migration and invasion assays.

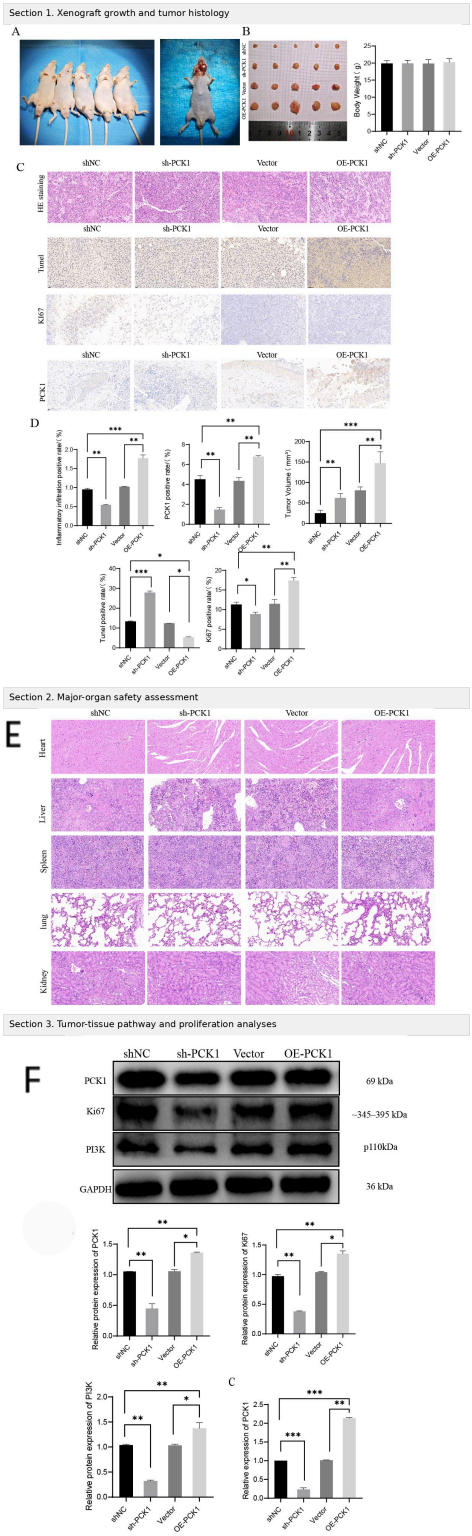



**Figure 4**

Xenograft, histological, major-organ, and tumor-tissue protein analyses following PCK1 manipulation. Groups are labeled sh-PCK1, shNC, Vector, and OE-PCK1. (A, B) Representative mice, excised tumors, body-weight assessment, and tumor-burden comparisons. (C, D) Tumor H&E staining, TUNEL analysis, and PCK1 and Ki67 immunohistochemistry with quantitative comparisons. (E) H&E staining of the heart, liver, spleen, lung, and kidney. (F) Immunoblotting and densitometric analyses of PCK1, Ki67, total PI3K, and GAPDH.

## Supplementary Files

This is a list of supplementary files associated with this preprint. Click to download.

- Supplementarymaterial.7z